Contents lists available at ScienceDirect

Solid State Ionics

Scalable synthetic method for SOFC compounds

A. Wain-Martin[a],[*], A. Morán-Ruiz[a], K. Vidal[a], A. Larrañaga[a], M.A. Laguna-Bercero[b], M.I. Arriortua[a],[c],[**]

[a] Universidad del País Vasco (UPV/EHU), Facultad de Ciencia y Tecnología, Barrio Sarriena S/N, 48940 Leioa, Vizcaya, Spain
[b] CSIC-Universidad de Zaragoza, Instituto de Ciencia de Materiales de Aragón (ICMA), Pedro Cerbuna 12, 50009 Zaragoza, Spain
[c] BCMaterials, Parque Tecnológico de Zamudio, Ibaizabal Bidea, Edificio 500-Planta 1, 48160 Derio, Spain

ARTICLE INFO

ABSTRACT

Although economically competitive SOFC systems seems to be ready for commercialization, a broad inventory of key starting materials and fabrication processes are needed to enhance systems and reduce costs. These necessities are raised by the demands for large scale SOFC industrial production. Taking into account these reasons, we have synthesized the mean components of a fuel cell, on a large scale, by the glycine nitrate combustion method.

The synthesized different components of SOFC have been the interconnector protective coating ($MnCo_{1.9}Fe_{0.1}O_4$), contact layer ($LaNi_{0.6}Fe_{0.4}O_3$), cathode ($La_{0.6}Sr_{0.4}FeO_3$), interlayer ($Sm_{0.2}Ce_{0.8}O_{1.9}$), electrolyte ($(ZrO_2)_{0.92}(Y_2O_3)_{0.08}$) and anode ($Ni_{0.3}O$-$(ZrO_2)_{0.92}(Y_2O_3)_{0.08}$) material, obtaining reproducible pure samples and amounts up to 12 g for each batch, being able to increase easily this amount to lots of hundred of grams.

The obtained materials have been characterized by inductively coupled plasma atomic emission spectroscopy (ICP-AES) and X-ray fluorescence (XRF), X-ray diffraction (XRD), dilatometry, scanning electron microscopy (SEM), particle size distribution and conductivity measurements.

1. Introduction

New kind of necessities arises from the development of technologies used in synthesis of SOFC materials. These necessities are originated from the demands for appropriate industrial production procedure of SOFC materials, and the respective final products. Therefore, Combustion Synthesis (CS) is an important method for advanced SOFC component fabrication, because is economical and energy efficient method [1].

CS methods can be classified into three categories, on the basis of the physical nature of reaction mixture itself: (i) flame synthesis or gas phase combustion, (ii) heterogeneous condensed phase combustion synthesis and (iii) solution combustion synthesis (SCS) [2]. Focusing in the SCS route, it consists of using an oxidizer (generally metal nitrates) and a suitable organic fuel (urea, citric acid, glycine, etc.) [3,4]. In this sense, SCS represents an exothermic method, which can provide enough energy to evaporate volatile impurities as well as, for the complete calcination of the products, producing, by a single step, pure nanostructured and homogeneous oxide powders with appropriate microstructural properties [5,6].

The major parameters such as fuel mixture and fuel/oxidizer ratio can play a significant role on phase formation of different compounds [7]. The choice of organic fuel (usually glycine, urea, sucrose, citric acid or alanine) is important because different fuels have different properties such as decomposition temperature, heat of combustion and reducing valency [8]. In general, a good fuel should react non violently, producing non toxic gases, an reacting as a complexant for metal cations [9]. As consequence, glycine was selected as the fuel since it is more cost-effective, has demonstrate that can be conveniently employed to prepare ceramic powders and its combustion heat (-3.24 kcal g^{-1}) is greater than that of urea (-2.98 kcal g^{-1}) or citric acid (-2.76 kcal g^{-1}), being more stronger complexing agent and forming stable gels in nitrate solution [9–12]. The advantages of the glycine nitrate combustion process are relatively low cost, fast heating rates, short reaction times, high composition homogeneity and high energy efficiency [13].

The commonly used materials for fuel cell devices are porous cermets of metallic NiO-$(ZrO_2)_{0.92}$ $(Y_2O_3)_{0.08}$ (NiO-YSZ) as an anode and dense $(ZrO_2)_{0.92}$ $(Y_2O_3)_{0.08}$ (YSZ) layers as electrolyte [14–16]. According to other authors and to our previous studies, $La_{0.6}Sr_{0.4}FeO_3$ (LSF40) has demonstrated to be a practical cathode using $Sm_{0.2}Ce_{0.8}O_{1.9}$ (SDC) as barrier between cathode and electrolyte,

avoiding poorly conducting secondary phases which increases contact resistance of the system [17–20]. Earlier studies have concluded that the use of $LaNi_{0.6}Fe_{0.4}O_3$ (LNF60) cathode contact layers improves electrons transfer through the contact interface from interconnect to active cathode layer [21,22]. Also, $MnCo_{1.9}Fe_{0.1}O_4$ (MCF10) can be used as an interconnect protective coating to avoid the Cr poisoning to the cathode [23,24].

The present work presents the adaptation of an existing lab-scale cell components production method to an industrially ready and easily scalable method using glycine-nitrate combustion synthesis. After the synthesis optimization, up to 12 g of sample have been obtained in each batch. The synthesized components were: anodes, electrolytes, interlayers, cathodes, contact layers and interconnect protective coatings. Therefore, results of a complete characterization study have been reported including compositional identification of phases, crystal structure, electrical and ionic conductivity, thermal expansion and morphological structure, showing a good reproducibility in all the cases.

2. Experimental

2.1. Powder preparation

All the SOFC component powders were prepared by a glycine nitrate process (GNP). Stoichiometric amounts of the corresponding metal nitrates, which were chosen because their low price under 2.90 € per gram, were dissolved in deionized water (see Table 1), to yield 36 g of the final oxide powders.

For all compositions glycine was then added into the nitrate aqueous solution while stirring. In all the cases a glycine nitrate molar ratio of 1 was used. The effect of different glycine nitrate ratio was previously analyzed for these kind of compounds in the research group [5]. The resulting viscous liquid was auto-ignited by heating up to approximately 455 °C. The obtained powders were calcined between 600 and 800 °C for 5 h to remove carbon residues. In the case of LSF40, LNF60 and MCF10, the resulting powders were pelletized and calcined in air at 950 °C for 8 h, which after several test, demonstrated to be the most economical treatment conditions to obtain pure samples.

2.2. Characterization techniques

Compositional analysis was performed for all the prepared samples to confirm that the expected elemental composition was achieved. The metal contents of Mn, Co, Fe, Sr, Ni and La, were determined by inductively coupled plasma atomic emission spectroscopy (ICP-AES) on a Horiba Yobin Yvon Activa spectrophotometer. Because their difficulty to dissolve, the analysis of Sm, Ce, Zr and Y contents were carried out with X-ray fluorescence (XRF) on a Fischercope X-ray XDAL.

Room-temperature X-ray diffraction (XRD) data were recorded using an integration time of 10s/0.026° step in the $5 < 2\sigma < 70°$ range with a Philips X'Pert-PRO X-ray diffractometer equipped with a secondary beam graphite monochromated and Cu-Kα radiation.

The morphologies of the powder samples were observed using a scanning electron microscope (JEOL JSM-7000F). Secondary electron images were taken at 20 kV and $1 \cdot 10^{-11}$ A, using a working distance of 8 mm. Particle size distribution of the powders was carried out using a Mastersizer particle size analyzer (Malvern Instruments). All the measurements were done using isopropanol as dispersion medium and using ultrasounds to break up the agglomerates that are formed.

To measure bulk conductivity and thermal expansion coefficient (TEC), pellets of the powders were sintered between 1050 and 1350 °C, and then, cut in $1 \times 3 \times 7$ mm bars. The bulk density of each sample was calculated by measuring the mass and the dimensions of the bars. The samples had a density of around 75% of the theoretical (X-ray) density.

DC conductivity measurements were performed in air by the four-point DC method using a VSP potentiostat controlled by PC using Lab Windows/CVI field point system.

Electrical contacts were made using Pt wires and Pt paste placed over whole end faces ensuring a homogeneous current flow. Voltage contacts were made as small as possible to avoid any disturbance of the contacts on the current flow. Measurements were performed from 450 to 950 °C. The conductivity (σ) was determined from a set of V-I values by taking $\sigma = 1/\rho = L/A \times dI/dV$, where L is the distance between voltage contacts and A is the sample cross section. Finally, TEC measurements were carried out from room temperature to 950 °C in air with a heating rate of 5 °C/min by using a Unitherm Model 1161 dilatometer system (Anter Corporation PA 15235).

3. Results and discussion

3.1. Elemental composition

In order to be able to study the reproducibility of large-scale synthesis of used compounds, three different synthesis have been perform for each compound, labeling as batch the 12 g of product gained in each synthesis. The nominal composition of the samples and the results from the ICP-AES analysis are shown in Table 2.

Within the experimental errors for all the samples, the experimental compositional values match the nominal composition.

Because the difficulties to dissolve SDC, NiO-YSZ and YSZ samples, the compositional measurements of these samples has been performed by XRF technique. The results are shown in the Table 3.

The results obtained by XRF analysis (Table 3) were close to the nominal values for all the studied samples. In all the cases, the difference between the relative amounts of the elements in different batches was not significant. Thus, the synthesis procedure shows an adequate chemical reproducibility.

3.2. Structural study

The purity of the samples was studied by X-ray diffraction. All the materials (LSF40, LNF60, MCF10, SDC, NiO-YSZ and YSZ) prepared through the glycine nitrate (GN) combustion route present the desired final phases. For the LNF60 compound, the appearance of extra shoulders in the experimental profile indicates a possible phase segregation to give two perovskite phases with different Ni/Fe ratio. In the NiO-YSZ case, the diffractogram presents peaks relative to the phases of NiO and YSZ (cubic structure), which evidences that the materials did

Table 1
Summary of used starting materials.

Compound	Starting materials[a]
$La_{0.6}Sr_{0.4}FeO_3$ (LSF40)	$La(NO_3)_3 \cdot 6H_2O$ (> 99%), $Sr(NO_3)_2$ (> 99%) and $Fe(NO_3)_2 \cdot 9H_2O$ (> 98%)
$LaNi_{0.6}Fe_{0.4}O_3$ (LNF60)	$La(NO_3)_3 \cdot 6H_2O$ (> 99%), $Ni(NO_3)_2 \cdot 6H_2O$ (> 98.5%) and $Fe(NO_3)_2 \cdot 9H_2O$ (> 98%)
$MnCo_{1.9}Fe_{0.1}O_4$ (MCF10)	$Mn(NO_3)_2 \cdot xH_2O$ (> 98%), $Co(NO_3)_2 \cdot 6H_2O$ (> 98%) and $Fe(NO_3)_3 \cdot 9H_2O$ (> 98%)
$Sm_{0.2}Ce_{0.8}O_{1.9}$ (SDC)	$Sm(NO_3)_3 \cdot 6H_2O$ (> 99.9%) and $Ce(NO_3)_3 \cdot 6H_2O$ (> 99%)
$Ni_{0.3}O-(ZrO_2)_{0.92}(Y_2O_3)_{0.08}$ (NiO-YSZ)	$Y(NO_3)_3 \cdot 6H_2O$ (> 99.9%), $ZrO(NO_3)_2 \cdot xH_2O$ (> 99%) and $Ni(NO_3)_2 \cdot 6H_2O$ (> 98.5%)
$(ZrO_2)_{0.92}(Y_2O_3)_{0.08}$ (YSZ)	$Y(NO_3)_3 \cdot 6H_2O$ (> 99.9%) and $ZrO(NO_3)_2 \cdot xH_2O$ (> 99%)

[a] All the starting materials used were from Sigma-Aldrich.

Table 2
Summary ICP results for LSF40 (La, Sr, Fe), LNF60 (La, Ni, Fe) and MCF10 (Mn, Co, Fe).

	Sr	La	Fe	Ni	Mn	Co
LSF40 (Batch 1)	0.41 (1)	0.58 (2)	1.02 (3)	–	–	–
LSF40 (Batch 2)	0.40 (1)	0.58 (2)	1.01 (3)	–	–	–
LSF40 (Batch 3)	0.41 (1)	0.58 (2)	1.02 (3)	–	–	–
LNF60 (Batch 1)	–	0.98 (9)	0.41 (6)	0.61 (8)	–	–
LNF60 (Batch 2)	–	0.97 (9)	0.41 (6)	0.60 (8)	–	–
LNF60 (Batch 3)	–	1.02 (9)	0.45 (6)	0.65 (8)	–	–
MCF10 (Batch 1)	–	–	0.10 (1)	–	0.99 (4)	1.86 (5)
MCF10 (Batch 2)	–	–	0.10 (1)	–	1.02 (4)	1.90 (5)
MCF10 (Batch 3)	–	–	0.10 (1)	–	0.98 (4)	1.93 (5)

Table 3
Summary XRF results for SDC (Sm, Ce), NiO-YSZ (Ni, Y, Zr) and YSZ (Y, Zr).

	Zr	Y	Ni	Sm	Ce
SDC (Batch 1)	–	–	–	0.8 (1)	0.3 (2)
SDC (Batch 2)	–	–	–	0.8 (1)	0.3 (2)
SDC (Batch 3)	–	–	–	0.8 (1)	0.3 (2)
NiO-YSZ (Batch 1)	0.8 (3)	0.2 (1)	0.3 (4)	–	–
NiO-YSZ (Batch 2)	0.8 (3)	0.2 (1)	0.3 (4)	–	–
NiO-YSZ (Batch 3)	0.8 (3)	0.2 (1)	0.3 (4)	–	–
YSZ (Batch 1)	0.8 (9)	0.2 (3)	–	–	–
YSZ (Batch 2)	0.8 (9)	0.2 (3)	–	–	–
YSZ (Batch 3)	0.8 (9)	0.2 (3)	–	–	–

Fig. 1. X-ray diffraction patterns measured of (a) LSF40, LNF60, MCF10, (b) SDC, NiO-YSZ and YSZ.

not react at these temperatures. The signal identification for all XRD patterns is in good agreement with the Power Diffraction File database (PDF) [25]. All the syntheses are reproducible and pure as can be

Table 4
Crystallite sizes of the synthesized compounds.

Batch	Compound (h,k,l)	Crystallite size (nm)	FWHM	Compound (h,k,l)	Crystallite size (nm)	FWHM
1	YSZ (1,1,1)	6 (2)	1.52	LSF40	46 (2)	0.28
2		6 (2)	1.53	(1,0,4)	45 (2)	0.28
3		6 (2)	1.55		45 (2)	0.28
1	SDC (1,1,1)	15 (1)	0.65	LNF60	16 (1)	0.60
2		15 (1)	0.64	(1,0,4)	17 (1)	0.59
3		14 (1)	0.67		16 (1)	0.60
1	NiO-YSZ	5 (1)	1.70	MCF10	182 (5)	0.14
2	(1,1,1)	5 (1)	1.70	(3,1,1)	186 (5)	0.14
3		5 (1)	1.70		189 (5)	0.14
1	NiO (2,2,0)	10 (1)	1.00			
2		11 (1)	0.87			
3		10 (1)	0.99			

observed in Fig. 1 for different batches.

The used synthetic temperatures indicate an absence of reactivity or decomposition of the starting materials under SOFC operating conditions (800 °C).

In order to obtain information about the crystal size of the synthesized powders, the Scherrer formula has been used (Table 4). The Scherrer equation relates the width of a powder diffraction peak to the average dimensions of crystallites in a polycrystalline powder (the used instrumental contribution is of 0.1 and the shape factor of 0.9).

As it can be seen, crystallite sizes are homogeneous between different batches of the same compound, showing crystal grown reproducibility.

3.3. Microstructure

Fig. 2 represents the SEM images for all the synthesized powders. In the case of LSF40, LNF60, MCF10 and SDC, well-necked morphologies of the powders synthesized by the combustion method and sintered at 950 °C are shown (a, b, c and d, respectively), which are composed of nanosized particles and agglomerations of grains of small number of micrometers.

The micrographs of the obtained samples of NiO-YSZ and YSZ are shown in Fig. 2 (e and f, respectively). Nano-sized particles are obtained, morphologically homogeneous and uniformly porous. In these cases, because of a large amount of the outcoming gases as-prepared samples are rather voluminous and very fragile. The particles are bound together into agglomerates of different shapes and sizes of a few micrometers.

In all the cases, the agglomerates formed during the combustion reaction are usually soft and easy to break due to the higher escaping gases for these samples [5]. In addition, comparing the same compound between different batches, it can be shown that the particle sizes and shapes are homogeneous. In addition, they are very microstructurally suitable starting materials to be used in the manufacture of SOFCs.

Particle size distribution of these materials has been measured for their manufacturing in SOFCs since this parameter influences the rheological properties for their deposition by wet colloidal spraying, after a ball milling with isopropanol.

As it is shown in Fig. 3, the aggregate sizes are homogeneous between different batches demonstrating that the synthesis is reproducible concerning the final processing sizes. Table 5 summarizes the details.

3.4. Electrical conductivity

The electronic conductivity of LSF40 and Ni-YSZ, can be described by the thermally activated small polaron mechanism [26,27] which is generally expressed as (Eq. (1)):
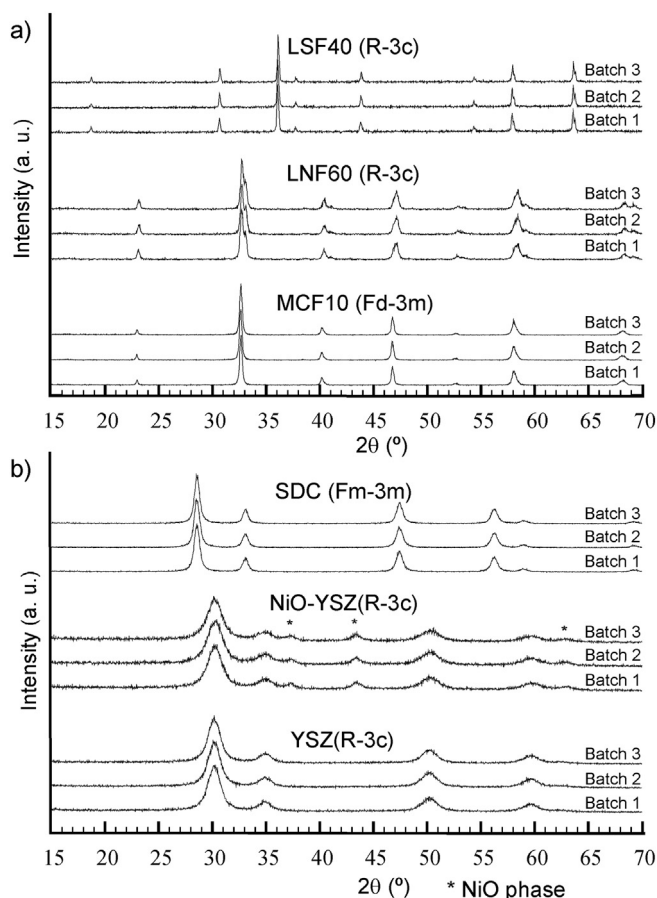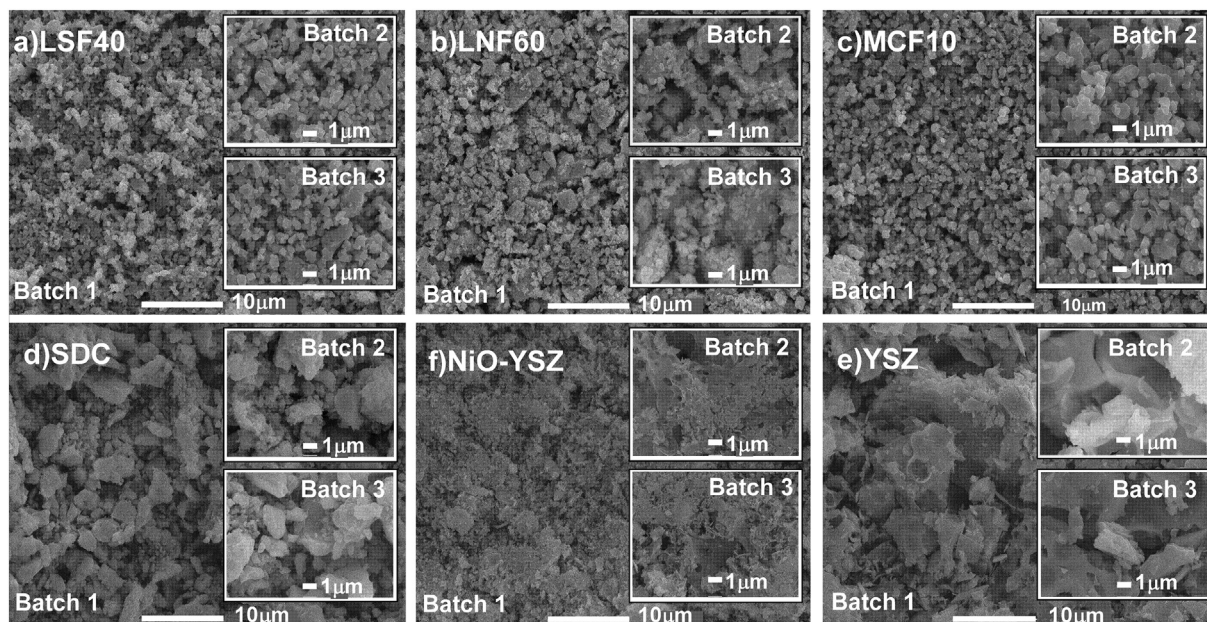
Fig. 2. SEM micrographs of the powder samples of a) LSF40, b) LNF60, c) MCF10, d) SDC, e) NiO-YSZ and f) YSZ.

$$\sigma = A/T\ \exp(-Ea/kT) \qquad (1)$$

In which E_a is the activation energy for small polaron hopping conduction, k is the Boltzmann constant, T is the absolute temperature and A is a pre-exponential factor independent of the temperature.

Taking into account the obtained relative density values, the porosity of the samples has to be considered in further analysis of the electric conductivity. So, for the two-phase systems (electrically conductive and nonconductive (porosity) phases), the corrected electrical conductivity was calculated using Eqs. (2) and (3) [18]:

$$\sigma_{corrected} = \sigma_{measured}\left(1 + (P_{fvol}/1 - (p_{fvol})^{2/3})\right) \qquad (2)$$

$$P_{fvol} = 1 - (\rho_{exp}/\rho_{theor}) \qquad (3)$$

where ρ_{exp} is the experimental geometric density of a pelletised sample and ρ_{theor} the theoretical density from XRD measurements. Note that the relative density, $(\rho_{exp}/\rho_{theor})$, could be slightly underestimated because the formula weight used in the ρ_{theor} calculation ignores oxygen vacancies.

In the case of LSF40, the conductivity increases with increasing temperature up to a maximum and then decreases due to the lattice
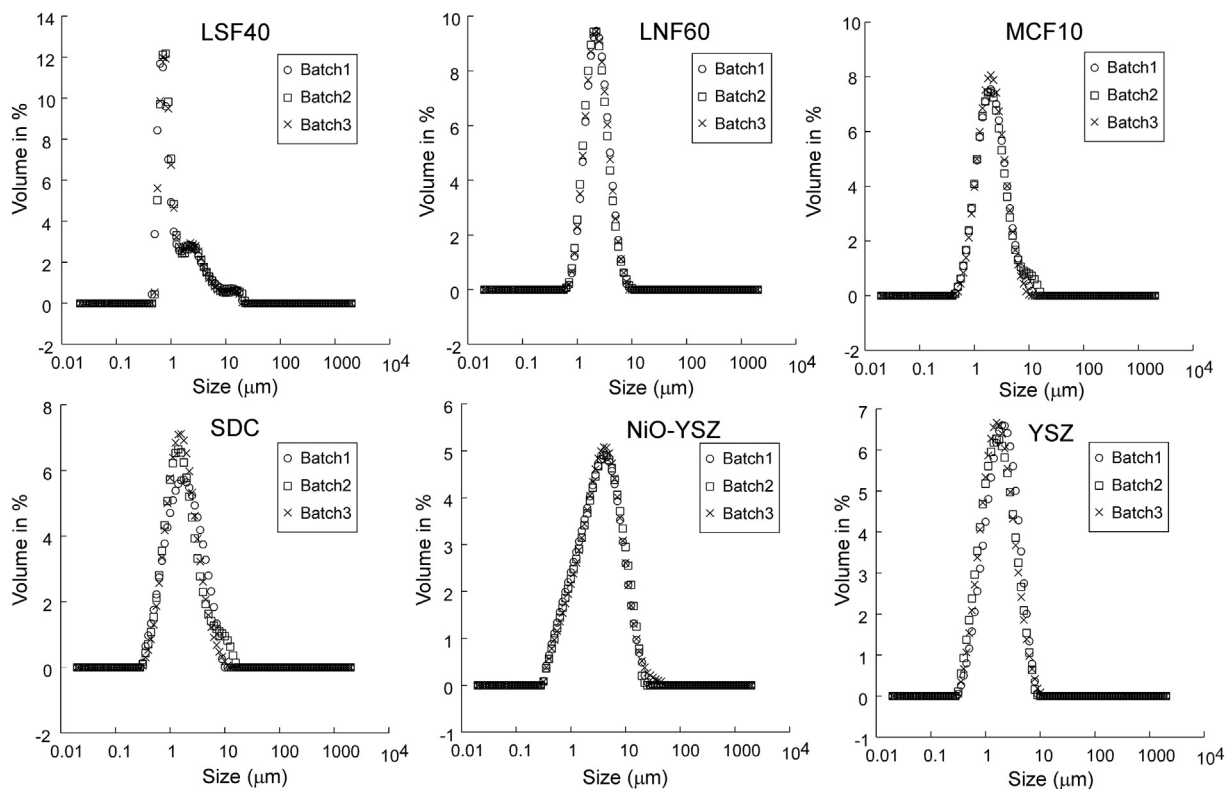

Fig. 3. Particle size distribution curves for LSF40, LNF60 MCF10, SDC, NiO-YSZ and YSZ powders.

Table 5
Summary results of powders particle size distribution tests.

Compound	d (0.5 μm)	Compound	d (0.5 μm)
LSF40 (Batch 1)	0.903	SDC (Batch 1)	1.506
LSF40 (Batch 2)	0.902	SDC (Batch 2)	1.495
LSF40 (Batch 3)	0.960	SDC (Batch 3)	1.665
LNF60 (Batch 1)	2.161	NiO-YSZ (Batch 1)	3.293
LNF60 (Batch 2)	2.025	NiO-YSZ (Batch 2)	3.262
LNF60 (Batch 3)	2.063	NiO-YSZ (Batch 3)	3.260
MCF10 (Batch 1)	1.905	YSZ (Batch 1)	1.551
MCF10 (Batch 2)	1.913	YSZ (Batch 2)	1.371
MCF10 (Batch 3)	1.914	YSZ (Batch 3)	1.828

Table 6
Electrical conductivity values at different temperatures and activation energy.

Compound	NiO-YSZ	LSF40	LNF60	MCF10
σ (600 °C) (S/cm^{-1})	670	89	93	126
σ (700 °C) (S/cm^{-1})	617	74	87	168
σ (800 °C) (S/cm^{-1})	573	63	82	184
Ea (eV)	–	0.03	0.02	0.28

Table 7
Average TEC values of the obtained materials.

Component	Average TEC (200–800 °C) (1.10^{-6} °C^{-1})
Crofer 22APU	11.8 [22]
MCF10	14.6 (1)
LNF60	14.8 (0)
LSF40	15.8 (0)
SDC	14.4 (2)
YSZ	13.1 (2)
NiO-YSZ	13.3 (2)
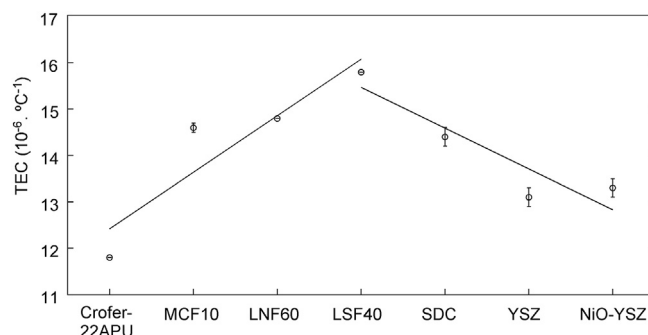
Fig. 5. TEC values obtained over the temperature range of 200–800 °C for all components.

oxygen loss, implying a small semiconductor behavior [22]. The electrical conductivity of MCF10 increases with increasing temperature. For the Ni-YSZ and LNF60 material, however, the conductivity decreases continuously with increasing temperature, implying a metallic behavior in the measured temperature range.

For comparison, electrical conductivities at different temperatures and activation energies for the oxygen ion transport of the different compounds have been represented in the Table 6.

The conductivity values obtained for the compounds are not comparable with the literature conductivity data ([22,24,28]), because these results are obtained on samples prepared using different chemical routes and/or calcined at different temperatures from ours, which may influence the size of the powder particles and the resultant grain size in sintered body [29,30].

3.5. Thermal expansion study

Thermal expansion coefficients are an important parameter for SOFCs. High temperature fuel cell stacks must meet the critical requirement that all layers have to retain good electrical contact, although large temperature changes occur at assembly and operating temperatures. In an ideal case, all materials would have the same thermal expansion coefficient (TEC), but in real configurations, differences will emerge that can cause thermo-mechanical stress. A further problem can occur because of the differences in the TECs of the different materials which result to a different change in thickness of the various layers and reduction of the system lifetime [31].

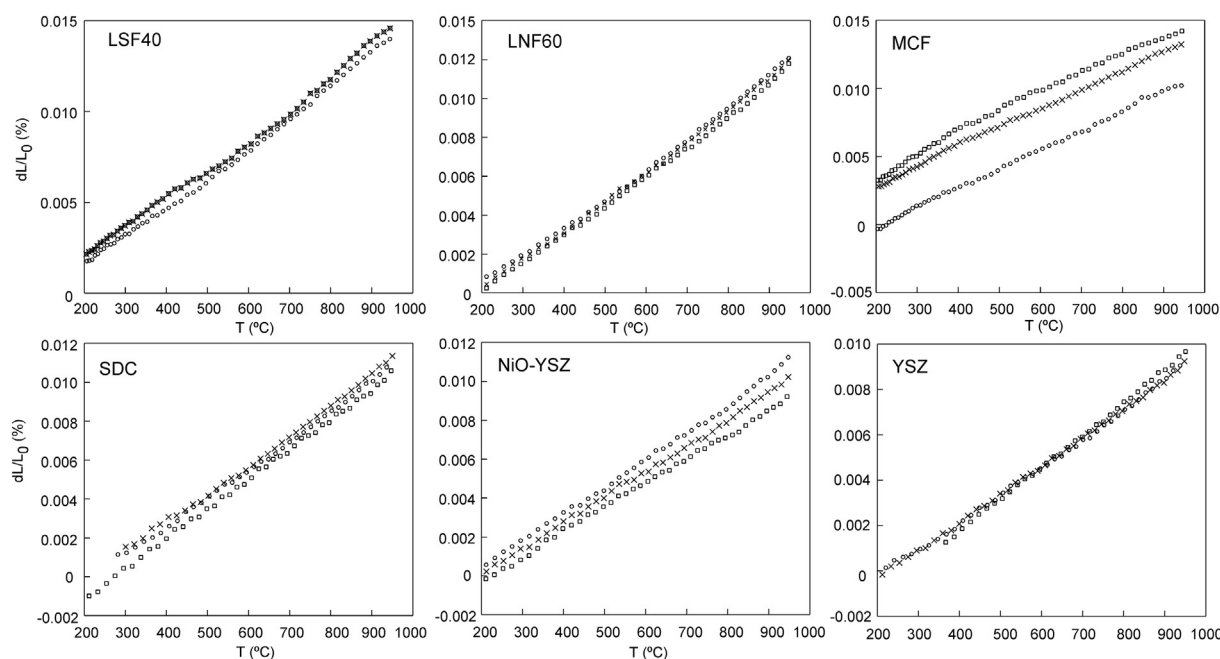Fig. 4 presents dilatometric curves of samples recorded between 200

Fig. 4. Thermal expansion behavior of components prepared by the combustion method.

and 950 °C in air that are almost linearly dependent on temperature. The value of the average lineal thermal expansion coefficients (TEC) of the compounds obtained over the temperature range of 200–800 °C are shown in Table 7.

The change in the thermal expansion coefficient between the different components is shown in Fig. 5.

As can be observed, the introduction of the corresponding layers between the electrolyte and cathode, and between the cathode and interconnector, minimizes the difference between their TEC values giving rise to similar values that are indicative of thermal compatibility, a factor which prevents failure due to stresses in SOFCs at high temperatures caused by thermal mismatches. Crofer-22APU interconnector has been included for a better TEC comparison between the adjacent compounds of MCF10 and NiO-YSZ. This material is the one that was analyzed as interconnect material for this kind of SOFC synthesis by the research group [21,23].

4. Conclusions

An increase in the synthesized amount of compounds has been performed without complications, maintaining a suitable microstructure and purity for all studied materials.

Six different fuel cell compounds have been synthesized in big amounts by glycine-nitrate method with stoichiometric fuel/oxidizer ratio, obtaining high quality materials whose microstructural properties can be modified.

The achieved compounds have similar microstructures which limits the long time degradation for these kinds of multilayer systems.

The synthetic times are short, demonstrating to be compositionally and morphologically reproducible in different batches. Therefore, it can be concluded that the glycine-nitrate process, with an optimal G/N ratio of 1.0, is an appropriate technique for preparing big quantities of different compounds for SOFC fabrication.

References

[1] A. Kumar, A. Cross, K. Manukyan, R.R. Bhosale, L.J.P. van den Broeke, J.T. Miller, A.S. Mukasyan, E.E. Wolf, Combustion synthesis of copper–nickel catalysts for hydrogen production from ethanol, Chem. Eng. J. 278 (2015) 46–54.
[2] T. Wilberforce, A. Alaswad, A. Palumbo, M. Dassisti, A.G. Olabi, Advances in stationary and portable fuel cell applications, Int. J. Hydrog. Energy 41 (2016) 16509–16522.
[3] A. Kumar, A.S. Mukasyan, E.E. Wolf, Combustion synthesis of Ni, Fe and Cu multicomponent catalysts for hydrogen production from ethanol reforming, Appl. Catal. A Gen. 401 (2011) 20–28.
[4] A. Ecija, K. Vidal, A. Larrañaga, L. Ortega-San-Martin, M.I. Arriortua, Synthetic methods for perovskite materials. structure and morphology, in: Yitzhak Mastai (Ed.), Advances in Crystallization Processes, 19 2012, pp. 493–514 ISBN:978-953-51-0581-7.
[5] K. Vidal, A. Morán-Ruiz, A. Larrañaga, J.M. Porras-Vázquez, P.R. Slater, M.I. Arriortua, Characterization of LaNi$_{0.6}$Fe$_{0.4}$O$_3$ perovskite synthesized by glycine-nitrate combustion method, Solid State Ionics 269 (2015) 24–29.
[6] S.L. González-Cortés, F.E. Imbert, Fundamentals, properties and applications of solid catalysts prepared by solution combustion synthesis (SCS), Appl. Catal. A Gen. 452 (2013) 117–131.
[7] S. Rasouli, S.J. Moeen, Combustion synthesis of Co-doped zinc oxide nanoparticles using mixture of citric acid–glycine fuels, J. Alloys Compd. 509 (2011) 1915–1919.
[8] S. Singh, D. Singh, LaSrFeO$_4$ nanopowders synthesized by different combustion methods: effect of fuel/particle size, Ceram. Int. 42 (2016) 15725–15731.
[9] S. Hajarpour, K. Gheisari, A. Honarbakhsh Raouf, Characterization of nanocrystalline Mg$_{0.6}$Zn$_{0.4}$Fe$_2$O$_4$ soft ferrites synthesized by glycine-nitrate combustion process, J. Magn. Magn. Mater. 329 (2013) 165–169.
[10] K. Boobalan, A. Varun, R. Vijayaraghavan, K. Chidambaram, U.K. Mudali, Facile, scalable synthesis of nanocrystalline calcium zirconate by the solution combustion method, Ceram. Int. 40 (2014) 5781–5786.
[11] C.A. da Silva, N.F.P. Ribeiro, M.M.V.M. Souza, Effect of the fuel type on the synthesis of yttria stabilized zirconia by combustion method, Ceram. Int. 35 (2009) 3441–3446.
[12] R.K. Lenka, T. Mahata, P.K. Sinha, A.K. Tyagi, Combustion synthesis of gadolinia-doped ceria using glycine and urea fuels, J. Alloys Compd. 466 (2008) 326–329.
[13] W. Tuichai, P. Thongbai, V. Amornkitbamrung, T. Yamwong, S. Maensiri, Na$_{0.5}$Bi$_{0.5}$Cu$_3$Ti$_4$O$_{12}$ nanocrystalline powders prepared by a glycine–nitrate process: preparation, characterization, and their dielectric properties, Microelectron. Eng. 126 (2014) 118–123.
[14] H. Monzón, M.A. Laguna-Bercero, A. Larrea, B.I. Arias, A. Várez, B. Levenfeld, Design of industrially scalable microtubular solid oxide fuel cells based on an extruded support, Int. J. Hydrog. Energy 39 (2014) 5470–5476.
[15] R. Fernández-González, T. Molina, S. Savvin, R. Moreno, A. Makradi, P. Núñez, Fabrication and electrical characterization of several YSZ tapes for SOFC applications, Ceram. Int. 40 (2014) 14253–14259.
[16] Z. Wang, X. Huang, Z. Lv, Y. Zhang, B. Wei, X. Zhu, Z. Wang, Z. Liu, Preparation and performance of solid oxide fuel cells with YSZ/SDC bilayer electrolyte, Ceram. Int. 41 (2015) 4410–4415.
[17] A. Arregui, L.M. Rodriguez-Martinez, S. Modena, M. Bertoldi, J. van Herle, V.M. Sglavo, Stability of ferritic perovskite cathodes in anode-supported solid oxide fuel cells under different processing and operation parameters, Electrochim. Acta 58 (2011) 312–321.
[18] M. Tatko, M. Mosiałek, M. Dudek, P. Nowak, A. Kędra, E. Bielańska, Composite cathode materials Sm$_{0.5}$Sr$_{0.5}$CoO$_3$–La$_{0.6}$Sr$_{0.4}$FeO$_3$ for solid oxide fuel cells, Solid State Ionics 271 (2015) 103–108.
[19] K. Vidal, A. Larrañaga, A. Morán-Ruiz, A.T. Aguayo, M.A. Laguna-Bercero, M.P. Yeste, J.J. Calvino, M.I. Arriortua, Effect of synthesis conditions on electrical and catalytical properties of perovskites with high value of A-site cation size mismatch, Int. J. Hydrog. Energy 41 (2016) 19810–19818.
[20] K. Shimura, H. Nishino, K. Kakinuma, M.E. Brito, H. Uchida, Effect of samaria-doped ceria (SDC) interlayer on the performance of La$_{0.6}$Sr$_{0.4}$Co$_{0.2}$Fe$_{0.8}$O$_{3 − δ}$/SDC composite oxygen electrode for reversible solid oxide fuel cells, Electrochim. Acta 225 (2017) 114–120.
[21] A. Morán-Ruiz, K. Vidal, M.Á. Laguna-Bercero, A. Larrañaga, M.I. Arriortua, Effects of using (La$_{0.8}$Sr$_{0.2}$)$_{0.95}$Fe$_{0.6}$Mn$_{0.3}$Co$_{0.1}$O$_3$ (LSFMC), LaNi$_{0.6}$Fe$_{0.4}$O$_{3 − δ}$ (LNF) and LaNi$_{0.6}$Co$_{0.4}$O$_{3 − δ}$ (LNC) as contact materials on solid oxide fuel cells, J. Power Sources 248 (2014) 1067–1076.
[22] M.K. Stodolny, B.A. Boukamp, D.H.A. Blank, F.P.F. van Berkel, Impact of Cr-poisoning on the conductivity of different LaNi$_{0.6}$Fe$_{0.4}$O$_3$ cathode microstructures, Solid State Ionics 225 (2012) 136–140.
[23] V. Miguel-Pérez, A. Martínez-Amesti, M.L. Nó, A. Larrañaga, M.I. Arriortua, The effect of doping (Mn,B)$_3$O$_4$ materials as protective layers in different metallic interconnects for solid oxide fuel cells, J. Power Sources 243 (2013) 419–430.
[24] X. Montero, F. Tietz, D. Sebold, H.P. Buchkremer, A. Ringuede, M. Cassir, A. Laresgoiti, I. Villarreal, MnCo$_{1.9}$Fe$_{0.1}$O$_4$ spinel protection layer on commercial ferritic steels for interconnect applications in solid oxide fuel cells, J. Power Sources 184 (2008) 172–179.
[25] ICCD, Powder Diffraction File—Inorganic and Organic, Pennsylvania, USA, (1995).
[26] X. Pan, Z. Wang, B. He, S. Wang, X. Wu, C. Xia, Effect of Co doping on the electrochemical properties of Sr$_2$Fe$_{1.5}$Mo$_{0.5}$O$_6$ electrode for solid oxide fuel cell, Int. J. Hydrog. Energy 38 (2013) 4108–4115.
[27] M. Lubini, E. Chinarro, B. Moreno, V.C. de Sousa, A.K. Alves, C.P. Bergmann, Electrical properties of La$_{0.6}$Sr$_{0.4}$Co$_{1 − y}$Fe$_y$O$_3$ (y = 0.2–1.0) fibers obtained by electrospinning, J. Phys. Chem. C 120 (2016) 64–69.
[28] D.A. Osinkin, D.I. Bronin, S.M. Beresnev, N.M. Bogdanovich, V.D. Zhuravlev, G.K. Vdovin, T.A. Demyanenko, Thermal expansion, gas permeability, and conductivity of Ni-YSZ anodes produced by different techniques, J. Solid State Electrochem. 18 (2013) 149–156.
[29] Y. Ren, R. Küngas, R.J. Gorte, C. Deng, The effect of A-site cation (Ln = La, Pr, Sm) on the crystal structure, conductivity and oxygen reduction properties of Sr-doped ferrite perovskites, Solid State Ionics 212 (2012) 47–54.
[30] R.N. Basu, F. Tietz, E. Wessel, H.P. Buchkremer, D. Stöver, Microstructure and electrical conductivity of LaNi$_{0.6}$Fe$_{0.4}$O$_3$ prepared by combustion synthesis routes, Mater. Res. Bull. 39 (2004) 1335–1345.
[31] L. Blum, An analysis of contact problems in solid oxide fuel cell stacks arising from differences in thermal expansion coefficients, Electrochim. Acta 223 (2017) 100–108.